Transport Models for Double-Gate Metal Oxide Semiconductor Field Effect Transistor Simulation

Shih-Ching Lo[1], Jyun-Hwei Tsai[1], and Yiming Li[2,3]
[1]National Center for High-Performance Computing, Hsinchu 300, Taiwan
[2]Department of Nano Device Technology, National Nano Device Laboratories, Hsinchu 300, Taiwan
[3]Microelectronics & Information Systems Research Center, National Chiao Tung Univ., Hsinchu 300, Taiwan

Abstract: - Double-gate MOSFETs have been of great interest in these years. Simulation with drift-diffusion, hydrodynamic, Schrödinger-Poisson drift-diffusion, and density-gradient drift-diffusion models is performed to examine the model difference for double-gate MOSFETs. Different oxide thickness (T_{OX}), T_{OX} = 1.5, 2, 3, 4 nm, channel length, substrate doping concentration, and silicon film thickness are considered in this work. Device performance only can be estimated by using right transport model. In particular, there is a significant physical difference among the models for sub-100 nm double-gate MOSFETs.

Key-Words: - Quantum effects, Drift-Diffusion, Hydrodynamic, Schrödinger equation, Density Gradient, Double-gate Metal Oxide Semiconductor Field Effect Transistor.

1 Introduction

Double gate metal oxide semiconductor field effect transistor (DG-MOSFET) are of interest today mainly because of their inherent suppression of short-channel effects (SCEs), high transconductance and ideal subthreshold swing (S-swing) [1-6]. Thus, the scalability of semiconductor devices are intimated to nanoscale, where channel length (L_G) is less than 10 nm. Since DG-MOSFET it expected to be the possible technology of VLSI technology, characteristics of it, such as drain current (I_D), threshold voltage (V_{TH}), S-swing and speed, are studies [1-6]. Computer- aided simulation for semiconductors provides a software driven approach to explore new physics of new devices. Semiconductor device models, such as Drift-Diffusion (DD) and Hydrodynamic (HD) models, which describes the variation of energy and the effects of temperature on carrier transport, are the kernal of device simulation. Both the DD and HD models are the classical description of the transport physics of devices. In order to understand the characteristics of nanoscale devices, it is important to take quantum mechanical effects into account with the classical models [7-13].

For device engineering application, a quantitatively investigation of the quantum effects, oxide thickness, channel length, doping concentration and Si-film thickness on the drain current should be addressed. In this work, DG-MOSFETs with four oxide thickness, four channel lengths, four doping concentrations and four Si-film thickness are simulated systematically so as to discuss the variations of I_D quantitatively. Furthermore, the difference between classical and quantum mechanical models are compared by five models, which are DD, HD, Schrödinger-Poisson drift-diffusion (DD-SP), Density Gradient models (DD-DG and HD-DG) [14-16]. All simulated cases will be shown in detail later.

2 Modeling and Simulation

Drain current is simulated by the DD, HD, DD-SP, DD-DG and HD-DG models under different conditions. Before showing the simulated results, the models are described as the following subsections.

2.1 Classical Transport Models

DD and HD models are mentioned in this subsection. Firstly, the three governing equations of DD model are listed as follows. The Poisson equation is

$$\nabla \varepsilon \cdot \nabla \psi = -q\left(p - n + N_D - N_A\right), \quad (1)$$

where ε is the electrical permittivity, q is the elementary electronic charge, n and p are the electron and hole densities, and N_D and N_A are the number of ionized donors and acceptors, respectively. The other two equations are continuity equations, which are

$$q\frac{\partial n}{\partial t} - \nabla \cdot \mathbf{J_n} = -qR, \quad (2)$$

$$q\frac{\partial p}{\partial t} + \nabla \cdot \mathbf{J_p} = -qR, \quad (3)$$

where $\mathbf{J}_n = -qn\mu_n \nabla \phi_n$ and $\mathbf{J}_p = -qp\mu_p \nabla \phi_p$ are the electron and hole current densities. μ_n and μ_p are the electron and hole mobility, and ϕ_n and ϕ_p are the electron and hole quasi-Fermi potentials.

With continued scaling into the deep sub-micron regime, semiconductor devices can be described properly using the conventional DD model, which ignores velocity overshoot and overestimates the impact ionization generation rates. In this case, the HD model [7-8] provides a very good compromise. In the hydrodynamic model, the carrier temperatures T_n and T_p are not assumed to be equal to lattice temperature T_L, together with basic semiconductor equations, up to three additional equations can be solved to find the temperatures. In general, the model consists of the basic set of DD model and the energy conservation equations for electrons, holes and the lattice. The energy balance equations are as follows:

$$\frac{\partial W_n}{\partial t} + \nabla \cdot \mathbf{S_n} = \mathbf{J_n} \cdot \nabla E_C + \frac{dW_n}{dt}\Big|_{coll}, \tag{4}$$

$$\frac{\partial W_p}{\partial t} + \nabla \cdot \mathbf{S_p} = \mathbf{J_p} \cdot \nabla E_V + \frac{dW_p}{dt}\Big|_{coll}, \tag{5}$$

$$\frac{\partial W_L}{\partial t} + \nabla \cdot \mathbf{S_L} = \frac{dW_L}{dt}\Big|_{coll}, \tag{6}$$

where $\mathbf{J}_n = \mu_n \left(n\nabla E_C + k_B T_n \nabla n + f_n^{td} k_B n \nabla T_n - 1.5 n k_B T_n \nabla \ln m_e \right)$ and $\mathbf{J}_p = \mu_p \left(p\nabla E_V - k_B T_p \nabla p - f_p^{td} k_B p \nabla T_p - 1.5 p k_B T_p \nabla \ln m_h \right)$ are current densities. E_C and E_V are the conduction and valence band energies, respectively. The first term takes into account the contribution due to the spatial variations of electrostatic potential, electron affinity, and the band gap. m_e and m_h are the effective masses of electron and hole. The energy fluxes are $\mathbf{S_L} = -\kappa_L \nabla T_L$, $\mathbf{S_n} = -5 r_n \left(\mathbf{J_n} k_B T_n / q + f_n^{td} \hat{\kappa}_n \nabla T_n \right) / 2$ $\mathbf{S_p} = -5 r_p \left(\mathbf{J_p} k_B T_p / q + f_p^{td} \hat{\kappa}_p \nabla T_p \right) / 2$, where

$$\hat{\kappa}_n = \frac{k_B^2}{q} n \mu_n T_n, \quad \hat{\kappa}_p = \frac{k_B^2}{q} p \mu_p T_p. \tag{7}$$

The collision terms are expressed by the following set of equations:

$$\frac{dW_n}{dt}\Big|_{coll} = -H_n - \frac{W_n - W_{n0}}{\tau_{en}}, \tag{8}$$

$$\frac{dW_p}{dt}\Big|_{coll} = -H_p - \frac{W_p - W_{p0}}{\tau_{ep}}, \tag{9}$$

$$\frac{dW_L}{dt}\Big|_{coll} = H_L + \frac{W_n - W_{n0}}{\tau_{en}} + \frac{W_p - W_{p0}}{\tau_{ep}}. \tag{10}$$

Here H_n, H_p, H_L and are the energy gain/loss terms due to generation/recombination processes. The expressions used for these terms are based on approximations made in [10]. The energy densities $W_n = nw_n = n(3k_BT_n/2)$ $W_p = pw_p = p(3k_BT_p/2)$ and $W_L = c_LT_L$. The corresponding equilibrium energy densities are $W_{n0} = nw_0 = n(3k_BT_L/2)$, $W_{p0} = pw_0 = p(3k_BT_L/2)$.

2.2 Quantum Mechanical Models

In principle, the Schröedinger equation coupled with classical model is the most accurate way to solve the carrier concentration, but it is not suitable for engineering applications. This is not only because it is computationally expensive but also because it is difficult to model the multi-dimensional cases. Therefore, researchers devote their efforts to develop quantum correction models, which produce a similar results to quantum mechanically calculated one but requires only about the same computation cost as that of the classical calculation.Because DG method is considered a better approximation than that of the Hänsch, van Dort model, and MLDA models [17-19], DG method is chosen in this work.

To include quantization effects in a classical device simulation, a simple approach is to introduce an additional potential, such as quantity Λ, in the classical density formula, which reads:

$$n = N_C \exp\left(\frac{E_F - E_C - \Lambda}{k_B T} \right), \tag{11}$$

where N_C is the conduction band density of states, E_C is the conduction band energy, and E_F is the electron Fermi energy. It is not possible to describe all quantum mechanical effects in terms of a variable Λ . For the SP-DD model, we include the quantization effects in the classical DD model by considering a Schrödinger equation along the semiconductor substrate (z - direction)

$$\left(-\frac{\partial}{\partial z} \frac{\hbar^2}{2m_{z,v}(z)} \frac{\partial}{\partial z} + E_C(z) \right) \Psi_{j,v}(z) = E_{j,v} \Psi_{j,v}(z). \tag{12}$$

Together with the 2DEG formula [11, 12, 13, 17-19] the Eq. (12) is introduced to the self-consistent DD model. $\hbar$ is the reduced Planck constant, E_C is the conduction band energy, v is the band valley, $m_{z,v}$, is the effective mass for valley in quantization direction, $\Psi_{j,v}$ is the j-th normalized eigenfunction in valley v; and , $E_{j,v}$ is the j-th eigenenergy. Solving the equations above, the device current can be directly

computed. On the other hand, Λ is given by Eq. (13) for the DG model.

$$\Lambda = -\frac{\gamma\hbar^2}{12m}\frac{\nabla^2\sqrt{n}}{\sqrt{n}}, \tag{13}$$

where $\hbar$ is the reduced Planck constant, m is the density of states mass, and γ is a fitting factor.

3 Results and Discussion

In the numerical studies, various DG-MOSFETs characteristics, which are four oxide thickness (T_{OX}), T_{OX} = 1.5, 2, 3, 4 nm, four channel length (L_G), L_G = 35, 65, 90 and 130 nm, four substrate doping concentration (N_A), $N_A = 1\times10^{17}$, 5×10^{17}, 1×10^{18}, and 5×10^{18} cm^{-3} and four Si-film thickness (H), H = 10, 20, 40, 65 nm, are considered to simulate by classical and quantum models. Numerical results of MOSFETs are simulated by ISE-DESSIS ver. 8.0.3 [20].

Figures 2 ~ 3 illustrate the simulated results of different doping concentration by classical and quantum mechanical models. As doping concentration increases, drain current decreases. It is because a heavy doping provides more charges in the substrate. Therefore, a heavy doping also results in a large threshold voltage. The varying percentages of drain current are discussed under the turn-on condition because of large fluctuation of subthreshold current. ΔI_D (%) is defined as $I_D(N_A) - I_D(5\times10^{18}\text{ cm}^{-3})] / I_D(5\times10^{18}\text{ cm}^{-3})$, where $N_A = 1\times10^{17}$, 5×10^{17} and 1×10^{18} cm^{-3}. According to Fig. 3, drain current varies largely with doping concentration. ΔI_D tends toward a stable percentage when current arrives the saturated current.

Simulated results of different Si-film thickness are shown in Figs. 4 ~ 5. ΔI_D (%) is defined as $I_D(H) - I_D(65\text{ nm})] / I_D(65\text{ nm})$, where H = 20, 40 and 65 nm. Drain current seems not being influenced by thickness of Si-film. The results are almost the same and the percentages of difference are within 10 % in turn-on region. However, the threshold voltage varies largely. H is smaller; threshold voltage is larger because of the shielding effects. Thus, employing a thin Si-film of DG-MOSFET can retard the SCE.

Next, the influence of channel length on drain current is discussed. It is found that short channel length induce large drain current. Obviously, as channel length becomes shorter, drain current becomes larger. From Figs 6 ~ 7, the increment increases as the channel length decreases. Due to the shielding-effect performed by the double-gate, which strongly reduces drain-induced barrier lowering (DIBL), the subthreshold current does not increase rapidly and roll-off of threshold voltage does not so sensitive to channel length scaling. To get insight into the influence of channel length, ΔI_D (%) is defined. $\Delta I_D = I_D(L_G) - I_D(130\text{ nm})] / I_D(130\text{ nm})$, where L_G = 35, 65 and 90 nm. Figure 7 is the comparison of different channel length in the turn-on region. Drain current is proportional to $1/L_G$. As channel length decreases 10 nm, a 0.1 mA/µm increase of drain current is observed. The increasing trend of classical and quantum are the same, however, the increasing rate of quantum cases is larger than classical cases.

The influence on oxide thickness on drain current are given in Figs. 8 ~ 9. The increase of I_D caused by oxide thickness scaling is proportional to the decrease of oxide thickness. Also, the influence is observed by ΔI_D (%), which is defined by $I_D(T_{OX}) - I_D(4\text{ nm})] / I_D(4\text{ nm})$, where T_{OX} = 1.5, 2 and 3 nm. A 0.5 mA/µm increase of drain current is observed when oxide thickness decreases 1 nm. Since oxide capacitance increases with oxide thickness scaling, threshold voltage decreases as T_{OX} decreases.

In addition, drain current simulated by different models are compared. From Fig. 10, I_D of HD is the largest and I_D of DD-DG is the smallest. That is, the temperature and energy effect enhance drain current and quantum effect reduce drain current. The result of DD-SP model is chosen as the comparing base. Comparing to HD and HD-DG models, DD, DD-DG and DD-SP models underestimated drain current. On average, a 70% ~ 60 % underestimation is observed. Therefore, the temperature and energy effect cannot be neglected. Also, the classical models overestimate drain current for 20 % ~ 30 %, especially when energy balance equations are considered. Drain currents simulated by DD, DD-DG and DD-SP are almost the same in this case. It is because the simulated channel length, which is 130 nm, and the oxide thickness, which is 4 nm, is not small enough to make quantum effect significantly. So as to understand the difference between classical and quantum effect under different physical condition, Figs. 12 ~ 13 are illustrated. The results of classical and quantum models have a 50 % difference in an extreme case. Generally, a 20 % overestimation of drain current by classical model is observed.

Although the DD model can be computed fast, it is not a good approximation of the quantum effects and the HD model. Since the difference of drain current for DD-DG and DD-SP model are insignificant, DD-DG model can be substituted for DD-SP model. The shielding effects of DG-MOSFET minimize the short channel effects and make drain current improvement with device scaling possible.

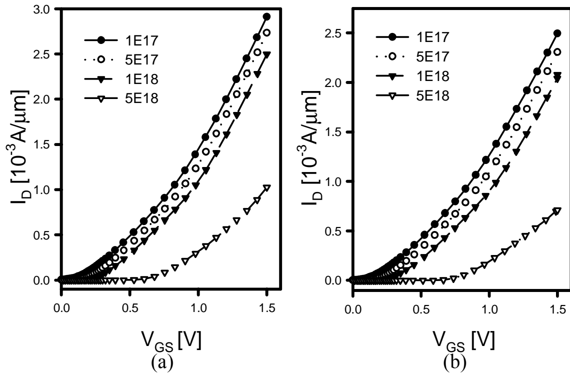

Fig. 2. Simulated I_D-V_{GS} curves for different doping concentration by the (a) DD model and (b) DD-DG model.

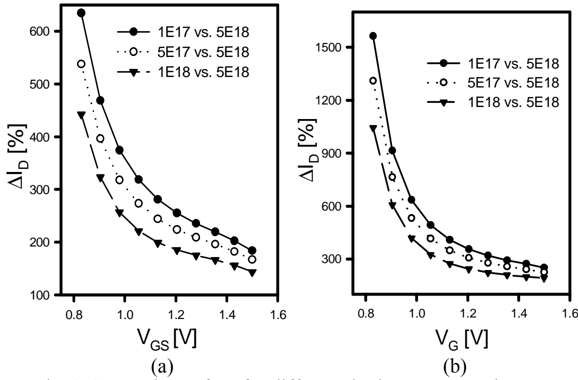

Fig. 3.Comparison of I_D for different doping concentration by the (a) DD model and (b) DD-DG model.

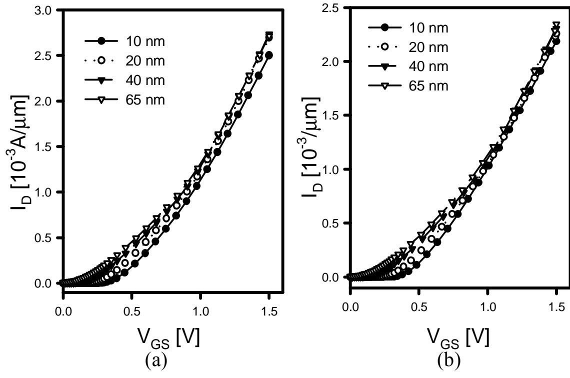

Fig. 4. Simulated I_D-V_{GS} curves for different Si-film thickness by the (a) DD model and (b) DD-DG model.

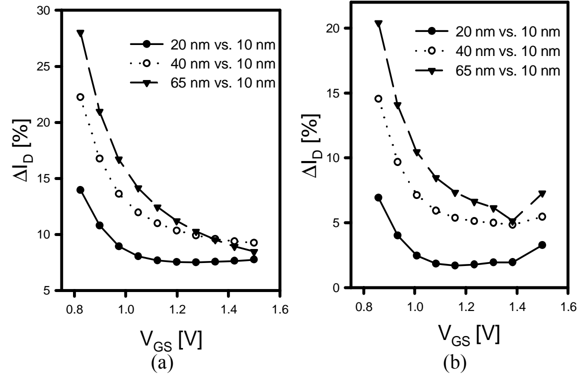

Fig. 5. Comparison of I_D for different Si-film thickness by the (a) DD model and (b) DD-DG model.

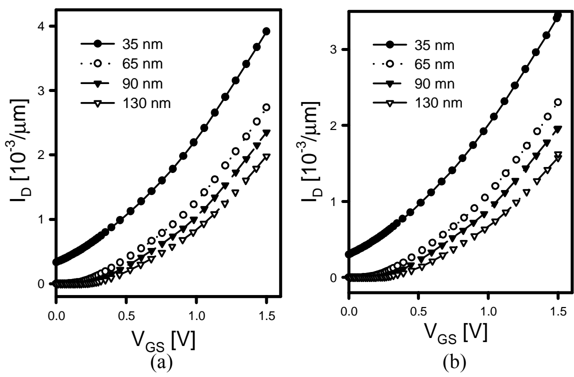

Fig. 6. Simulated I_D-V_{GS} curves for different channel length by the (a) DD model and (b) DD-DG model.

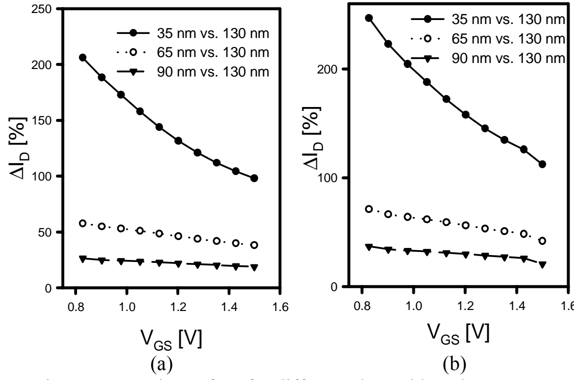

Fig. 7. Comparison of I_D for different channel length by the (a) DD model and (b) DD-DG model.

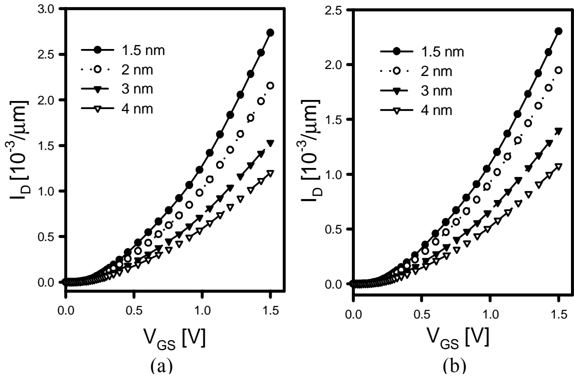

Fig. 8. Simulated I_D-V_{GS} curves for different oxide thickness by the (a) DD model and (b) DD-DG model.

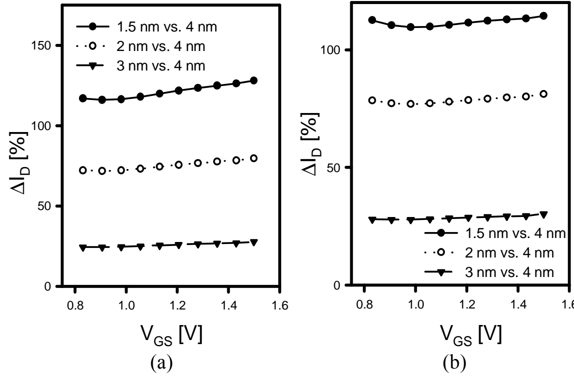

Fig. 9. Comparison of I_D for different oxide thickness by the (a) DD model and (b) DD-DG model.

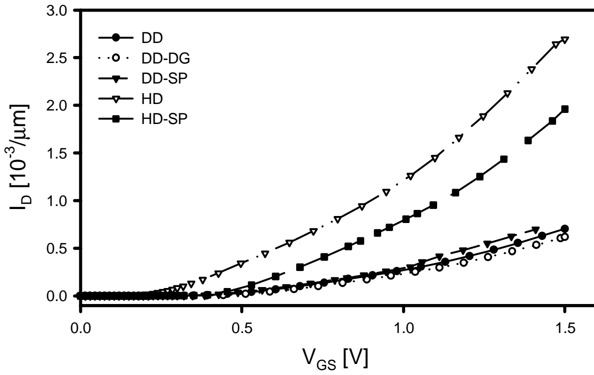

Fig. 10. Simulated I_D-V_{GS} curves for different models with L_G = 130nm, T_{OX} = 4 nm, H = 65 nm, N_D = 5E18.

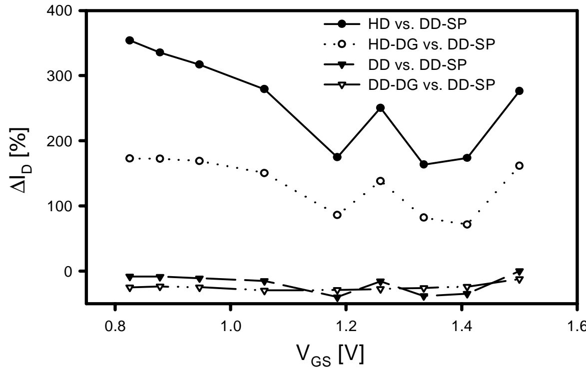

Fig. 11. Comparison of I_D for different models with L_G = 130 nm, T_{OX} = 4 nm, H = 65 nm, N_D = 5E18.

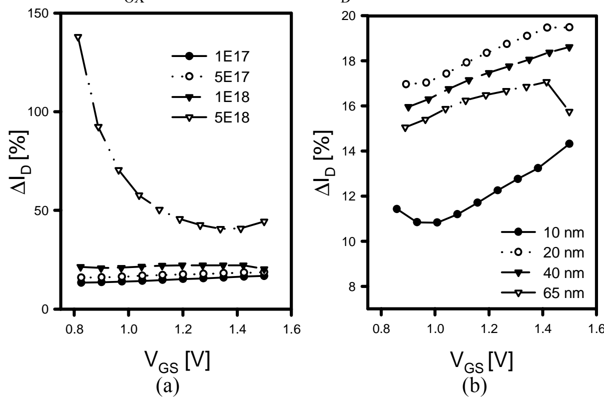

Fig. 12. Difference of I_D between classical and quantum models by (a) doping concentration and (b) Si-film thickness..

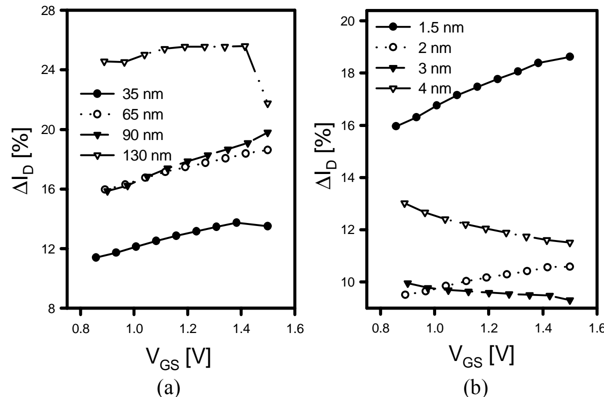

Fig. 13. Difference of I_D between classical and quantum models by (a) channel length and (b) oxide thickness..

4 Conclusions

In this paper, the numerical results of DD, HD, SP-DD and DG-DD models are examined so as to discuss the difference among the models quantitatively. DG-MOSFETs with four oxide thickness (T_{OX}), T_{OX} = 1.5, 2, 3, 4 nm, four channel length, four substrate doping concentration and four Si-film thickness are simulated by ISE-DESSIS ver. 8.0.3. According to the results, quantum and energy effects must be considered in the simulation of nanoscale devices. Scaling of DG-MOSFET surely make the continuous improvement in device performance without the drawback of SCE. However, there are still transport phenomena of DG-MOSFET to be analyzed, such as formation of inversion layer and electron density distribution. To understand DG-MOSFET well, 3-D simulation, which is left to future study, is necessary.

5 Acknowledgement

The work was partially supported by the National Science Council, Taiwan, R.O.C., under Contracts NSC – 92 – 2215 – E – 429 - 010, NSC – 92 – 2112 – M – 429 - 001, and NSC – 92 – 2815 – C – 492 – 001 - E. It was also partially supported by Ministry of Economic Affairs, R.O.C. under contract No. 91 – EC – 17 – A – 07 - S1 - 0011.

References:

[1] A. Rahman and M. S. Lundstrom, “A Compact Scattering Model for the Nanoscale Double-Gate MOSFET,” *IEEE Trans. Elec. Dev.*, Vol. 49, No. 3, pp.481-489, 2002.

[2] Y. Taur, “Analytical Solutions of Charge and Caacitance in Symmetric and Asymmetric Double-Gate MOSFETs,” *IEEE Trans. Elec. Dev.*, Vol. 48, No. 12, pp.2861-2869, 2001.

[3] D. Hisamoto, et al., “FinFET-A Self-Aligned Double-Gate MOSFET Scalable to 20nm,” *IEEE Trans. Elec. Dev.*, Vol. 47, No. 12, pp.2320-2325, 2000.

[4] H. S. P. Wong, K. K. Chen and Y. Taur, “Self-Aligned (Top and Bottom) Double-Gate MOSFET with a 25nm Thick Silicon Channel,” IEDM, pp.427-430, 1997.

[5] G. Baccarani and s. Reggiani, “A Compact Double-Gate Comparing Quantum -

Mechanical and Nonstatic Effects," *IEEE Trans. Elec. Dev.*, Vol. 46, No. 8, pp.1656-1666, 1999.
[6] Z. Ren, R. Venugopal, S. Goasguen, S. Datta and M. S. Lendstrom, "NanoMOS 2.5: A Two-Dimensional Simulator for Quantum Transport in Double-Gate MOSFETs," *IEEE Trans. Elec. Dev.*, Vol. 50, No. 9, pp.1914-1925, 2003.
[7] R. Stratton, "Diffusion of hot and cold electrons in semiconductor barriers," *Physics Review*, Vol. 126, No. 6, pp. 2002–2014, 1962.
[8] K. Bløtekjær, "Transport Equations for Electrons in Two-Valley Semiconductors," *IEEE Transactions on Electron Devices*, Vol. ED-17, No. 1, pp.38-47, 1970.
[9] T. W. Tang, "Extension of the Scharfetter-Gummel Algorithm to the Energy Balance Equation," *IEEE Transactions on Eletronic Devices*, Vol. 31, No. 12, pp.1912- 1914, 1984.
[10] D. Chen, et al., "Dual energy transport model with coupled latticeand carrier temperatures," *SISDEP-5*, (Vienna), pp. 157–160, Sept. 1993.
[11] Y. Li, "A Novel Approach to Carrier Temperature Calculation for Semiconductor Device Simulation using Monotone Iterative Method. Part I: Numerical Results," *Proc. 3rd WSEAS Symposium on Mathematical Methods Computing Technology Electrical Engineering (MMACTEE 2001)*, Athens, Dec. 2001, pp. 5721-5726.
[12] Y. Li, "A Novel Approach to Carrier Temperature Calculation for Semiconductor Device Simulation using Monotone Iterative Method. Part I: Numerical Algorithm," *Proc. 3rd WSEAS Symposium on Mathematical Methods Computing Technology Electrical Engineering (MMACTEE 2001),* Athens, Dec. 2001, pp. 5671-5676.
[13] Y. Li, S. M. Sze and T. S., Chao, "A Practical Implementation of Parallel Dynamic Load Balanceing for Adaptive Computing in VLSI Device Simulation," *Engineering with Computers*, Vol. 18, pp.124-137, 2002.
[14] M. G. Ancona and H. F. Tierstein, "Macroscopic Physics of the Silicon Inversion Layer," *Physical Review B*, Vol. 35, No. 15, pp.7959-7965, 1987.
[15] M. G. Ancona., "Nonlinear Discretization Scheme for the Density-Gradient Equations," *SISPAD'00,* pp.196-199, 2000.
[16] M. G. Ancona and H. F. Tierstein, "Full Macroscopic Description of Bounded Semiconductors with an Application to the $Si\text{-}SiO_2$ Interface," *Physical Review B*, Vol. 22, No. 12, pp.6104-6119, 1980.
[17] X. Wang, Quantum Correction to the Charge Density Distribution in Inversion Layers, MS. Thesis, University of Massachusetts, U. S. A., 2001.
[18] Y. Li, et al., "A Novel Parallel Approach for Quantum Effect Simulation in Semiconductor Devices," I*nternational Journal of Modelling and Simulation*, Vol. 23, No. 2, pp.1-8, 2003.
[19] Y. Li, et al., "A Novel Parallel Approach for Quantum Effect Simulation in Semiconductor Devices," I*nternational Journal of Modelling and Simulation*, Vol. 23, No. 2, pp.1-8, 2003.
[20] DESIS-ISE TCAD Release 8.0, *ISE integrated Systems Engineering AG*, Switzerland, 2002.